sciendo

Int. J. of Applied Mechanics and Engineering, 2019, vol.24, No.1, pp.67-77
DOI: 10.2478/ijame-2019-0004

INFLUENCE OF VISCOSITY ON THE SHAPE OF AN AIR TAYLOR BUBBLE IN A STAGNANT LIQUID UNDER TURBULENT CONDITION IN FALLING FILM

B. LERTNUWAT
Advanced Computational Fluid Dynamics Research Unit
Department of Mechanical Engineering
Faculty of Engineering, Chulalongkorn University
Bangkok, 10330 THAILAND
E-mail: Boonchai.L@Chula.ac.th

This work aims to find the influence of the liquid viscosity on the shape of an air Taylor bubble, rising up in a pipe column which contains the liquid under conditions that the liquid is stagnant and the Froude number is approximately equal to *0.35*. Five liquid viscosities (from *0.001* to *0.01* Pa·s) were selected for being computationally investigated. An appropriate shape of a Taylor bubble, corresponding to each selected viscosity, was obtained by considering a pressure distribution of the air inside the bubble. Simulation results showed that the Taylor bubble shape would be thicker if the liquid viscosity was decreased. This could be explained by using the theory of the log-law velocity profile.

Key words: Dumitrescu's model, viscosity, Taylor bubble, turbulence.

1. Introduction and theory

Over a range of intermediate flow rates of gas-liquid flows, a slug flow is sometimes formed. This kind of two-phase flows is interesting due to its unique characteristic, consisting of elongated gas bubbles and liquid slugs. It can be found in oil pipelines which connect the wells in seabed to oil refineries, in the geometrical power plant of steam, in the boiling or condensing of liquid-vapor power plants, in gas-liquid chemical reactors, in cooling systems of nuclear reactors and in very small transporting tubes of cryogenic. Because the slug flows can cause damages in the systems, such as the liquid slugs can cause a high momentum when the flows change direction in elbows or the low frequencies of the slug flows can induce a resonance in piping structures. There are many researchers trying to study behaviors of the slug flows. The shape of the elongated gas bubble (the so-called Taylor bubble) is a topic in which they are interested. According to [1], shapes of a Taylor may be predicted with

$$R_b = R_p\left[\frac{\Delta z}{R_p}\left(\frac{3}{2}-\frac{\Delta z}{R_p}\right)\right]^{\frac{1}{2}} \quad \text{when} \quad \Delta z \le 0.5R_p, \tag{1.1}$$

$$R_b = R_p\left[1 - Fr_D\left(\frac{R_p}{\Delta z}\right)^{\frac{1}{2}}\right]^{\frac{1}{2}} \quad \text{when} \quad \Delta z > 0.5R_p. \tag{1.2}$$

These equations were developed from Dumitrescu's model [2], derived with the potential flow theory. Because the potential flow theory neglects the influence of viscosity, both Eq.(1.1) and Eq.(1.2) predict the shape profiles of Taylor bubbles which are different from reality [1, 3-9].

A unit of the slug flow, shown in Fig.1, is usually employed for investigating the shape of a Taylor bubble. A slug flow unit is mainly comprised of a Taylor bubble, a liquid slug and a falling film. If an observer stands on the ground where a vertical pipeline is installed, he will see a Taylor bubble flowing upward in the stagnant liquid with a speed (w_b) with respect to the pipeline. However, for most of studies, the nose of the Taylor bubble is used as a reference frame and the liquid is instead considered as a moving part. Hence the liquid is considered to move downward with the speed (w_l) whose magnitude equals the magnitude of the Taylor bubble velocity, rising upward in the vertical pipe (w_b) in which the stagnant liquid is constained. In addition, they both can be related to the Froude number ($\mathrm{Fr_D}$) as follows.

$$w_b = w_t = \mathrm{Fr_D}\sqrt{gD_p} \ . \tag{1.3}$$

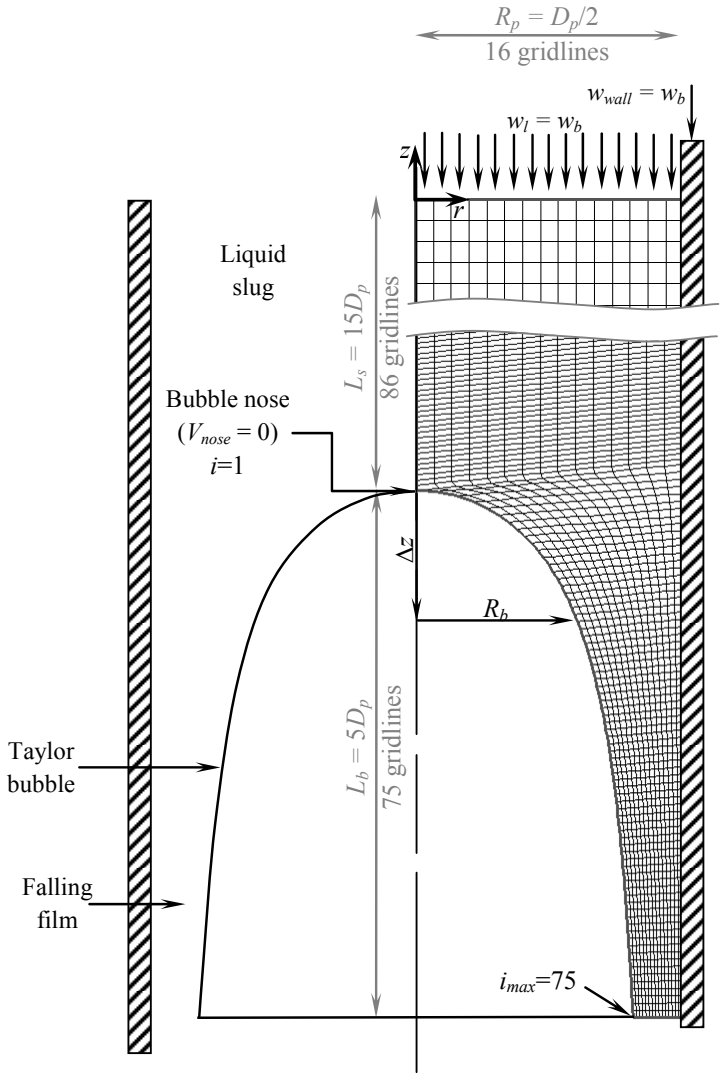

Fig.1. Schematic diagram of a liquid flow around a Taylor bubble in a stagnant liquid with respect to the Taylor bubble nose and an employed grid in a computational domain.

The Froude number in Eq.(1.3) is a function of Re_D and Eo_D, namely

$$\mathrm{Fr_D} = \sqrt{\frac{0.0089}{0.0725 + \frac{1}{\mathrm{Re}_D}\left(1 - 0.11\mathrm{Re}_D^{0.33}\right)}\left(1 + \frac{41}{\mathrm{Eo}_D^{1.96}}\right)^{-4.63}} \quad . \tag{1.4}$$

The formula was developed by [10] so that it agreed well with the data, obtained from the work of [11], and it overcomes inaccuracies at intermediate Morton numbers. According to Eq.(1.4), there are a few dimensionless numbers needed to be defined, i.e.

$$\mathrm{Re}_D = \frac{\rho_l w_t D_p}{\mu_l} \tag{1.5}$$

and

$$\mathrm{Eo}_D = \frac{\left(\rho_l - \rho_g\right) g D_p^2}{\sigma} . \tag{1.6}$$

Substitution of Eq.(1.3) into Eq.(1.5) yields

$$\mathrm{Re}_D = \frac{\rho_l \mathrm{Fr_D}\sqrt{gD_p^3}}{\mu_l} . \tag{1.7}$$

Then, substitution of Eq.(1.6) and Eq.(1.7) into Eq.(1.4) yields

$$\mathrm{Fr_D} = \sqrt{\frac{0.0089}{0.0725 + \frac{\mu_l}{\rho_l \mathrm{Fr_D}\sqrt{gD_p^3}}\left(1 - 0.11\left(\frac{\rho_l \mathrm{Fr_D}\sqrt{gD_p^3}}{\mu_l}\right)^{0.33}\right)}\left(1 + 41\left(\frac{\sigma}{\left(\rho_l - \rho_g\right) g D_p^2}\right)^{1.96}\right)^{-4.63}} \quad . \tag{1.8}$$

The obtained Eq.(1.8) shows that $\mathrm{Fr_D}$ is a function of D_p and fluid properties are (σ, ρ_g, ρ_l and μ_l). In order to investigate the influence of the liquid viscosity, μ_l will be varied while the other fluid properties and D_p must be fixed. Since air-water slug flows are often employed for studying in many research studies, the other properties of the fluids are assumed to be equal to those of air and water, namely $\sigma = 60.00 \times 10^{-3}$ *N/m*, $\rho_g = 1.18$ *kg/m*^{3} and $\rho_l = 1000$ *kg/m*^{3}. In this work, D_p was always equal to *0.05 m*. This is because air Taylor bubbles rising in stagnant water are found in pipes of which a diameter ranges from a very small size as capillary tubes to about *0.1 m* [*1*, *5*, *12-17*]. As a result, the average pipe diameter is approximately *0.05 m* and it is the size of the pipe in this work.

After substituting the abovementioned D_p, σ, ρ_g and ρ_l into Eq.(1.8), $\mathrm{Fr_D}$ will approach a maximum value (≈ 0.350) if μ_l is less or equal to *0.01* $\mathrm{Pa \cdot s}$. Since the viscosity of water approximately equals *0.001* $\mathrm{Pa \cdot s}$, μ_l will be varied between *0.001* and *0.01* $\mathrm{Pa \cdot s}$ in this work. Therefore, the objective of the work is to numerically investigate the influence of the liquid viscosity on the shapes of air Taylor bubbles in pipes, containing stagnant liquids under conditions that $\mathrm{Fr_D}$ is approximately equal to *0.350*.

2. Methodology and computational setup

Table 1 shows the 5 investigated conditions together with the corresponding values of the Reynolds number in the falling film region, namely

$$\mathrm{Re}_{film} = \frac{\rho_l \overline{w}_{film} \delta_{film}}{\mu_l} \approx \frac{\rho_l w_t D_p}{4\mu_l}. \tag{2.1}$$

The flow field around a Taylor bubble would be entirely laminar if Re_{film} is less than *250* in accordance with the results of [18]. Since, in this work, it was apparent that $\mathrm{Re}_{film} > 250$ for all cases as shown in Tab.1; a computational program code from [19] was employed. This program code was developed from the $k-\varepsilon$ model by using the implicit pressure-correction method on the finite volume framework with second order spatial accuracy in order to govern turbulent flows.

Table 1. Values of parameters for 5 investigating conditions.

μ_l ($\mathrm{Pa}\cdot\mathrm{s}$)	w_t (m/s)	$\mathrm{Fr_D}$	Re_D	Re_{film}	Eo_D	M
0.0100	*0.2454*	*0.3504*	*1227*	*307*	*408.8*	1.64×10^{-9}
0.0075	*0.2455*	*0.3505*	*1637*	*409*	*408.8*	5.17×10^{-10}
0.0050	*0.2455*	*0.3506*	*2455*	*614*	*408.8*	1.02×10^{-10}
0.0025	*0.2455*	*0.3505*	*4910*	*1227*	*408.8*	6.39×10^{-12}
0.0010	*0.2454*	*0.3504*	*12270*	*3068*	*408.8*	1.64×10^{-13}

According to the experimental results described in [5, 13, 20-21]; the averages of the slug length (L_s) and the Taylor bubble length (L_b) were respectively equal to $15\,D_p$ and $5\,D_p$. Therefore, these values were used to define the characteristic of the slug flow unit as shown in Fig.1. Besides the axis of symmetry along the pipe centerline allowed us to consider just half of the pipe. There were 16 gridlines on the *r*-axis, whereas the gridlines on the *z*-axis were divided in 2 parts, i.e. 86 gridlines were drawn from the centerline of the pipe and 75 gridlines were drawn from the Taylor bubble surface. A velocity inlet boundary condition was posed on the top of the domain with a fixed velocity (w_t), depending on the condition as shown in Tab.1. A pressure outlet condition was posed on the bottom of the domain with a fixed constant (p_l=*100k*Pa). A no-slip condition together with a wall function was posed along the pipe wall on the right side of the domain. Herein, the wall velocity (w_{wall}) was fixed to be w_t. A symmetry boundary condition was posed along the pipe centerline on the upper left side of the domain. And a free surface boundary condition was posed along the Taylor bubble surface on the lower left side of the domain. According to [22], shapes of the Taylor bubble surface (R_b) were created with

$$\frac{R_b}{D_p} = \frac{1}{2}\left[1-\left(\frac{\beta w_b^2+\delta}{2g\Delta z+\delta}\right)^{\frac{1}{2}}\right]^{\frac{1}{2}}, \tag{2.2}$$

$$\beta = a_1\left(1-e^{a_2\Delta z/D_p}\right). \tag{2.3}$$

The small constant δ was set to be 10^{-38}. It was added to avoid a singular point at $\Delta z = 0$. Both Eq.(2.2) and Eq. (2.3) show that the shape of a Taylor bubble could be adjusted with the values of α_1 and α_2 if D_p is known.

So far, a simulation of a flow around a Taylor bubble surface, created by Eq.(2.2) and Eq.(2.3) with specified values of α_1 and α_2, could be started. After the simulation, a pressure distribution of the liquid along the Taylor bubble surface would be obtained. This liquid pressure can be related to the gas pressure inside the Taylor bubble with

$$p_g\big|_{bs} = p_l\big|_{bs} + \sigma\frac{1}{R_{bs}} - 2\mu_l\left(\frac{\partial V_n}{\partial n}\right)_l\Bigg|_{bs}. \tag{2.4}$$

The radius of curvature (R_{bs}) could be calculated as follows

$$\frac{1}{R_{bs}} = \frac{1}{R_{bs1}} + \frac{1}{R_{bs2}} \tag{2.5}$$

where $R_{bs1} = -\left[1+\left(\frac{\partial z}{\partial r}\right)^2\right]^{\frac{3}{2}} \Big/ \frac{\partial^2 z}{\partial r^2}$ and $R_{bs2} = r\left[1+\left(\frac{\partial r}{\partial z}\right)^2\right]^{\frac{1}{2}}$.

The distribution of the gas pressure inside a Taylor bubble must be theoretically uniform. Hence, the values of α_1 and α_2 must be varied to adjust the Taylor bubble shape until the uniform pressure distribution of the gas inside a Taylor bubble was achieved. The root-mean-square derivation (RMSD) of residuals between the gas pressure at each data point along the Taylor bubble surface $\left(p_{g,i}\big|_{bs}\right)$ and the gas pressure at the Taylor bubble nose $\left(p_{g,nose}\big|_{bs}\right)$, i.e.

$$\mathrm{RMSD}_p = \sqrt{\left[\sum_{i=1}^{i_{\max}}\left(p_{g,i}\big|_{bs} - p_{g,nose}\big|_{bs}\right)^2 \Big/ \left(i_{\max}-1\right)\right]}, \tag{2.6}$$

was used to numerically judge how the obtained pressure distribution was uniform. As shown in Fig.1, the Taylor bubble nose locates at $i = 1$. While $i_{\max}$, which was equal to 75, is the maximum number of the data point along the Taylor bubble surface. It was clear that the value of RMSD_p will be equal to zero in the case of the uniform pressure distribution. However, the uniform pressure distribution was in practice difficult to be obtained so the minimum RMSD_p was chosen instead.

Since the values of α_1 and α_2 must be varied until they could create the appropriate shape of a Taylor bubble, the grid search method was exploited to find the appropriate values of α_1 and α_2. At the initial stage, a searching domain was assigned to be a range, bounded within $\alpha_{1\min,1} \le \alpha_1 \le \alpha_{1\max,1}$ and $\alpha_{2\min,1} \le \alpha_2 \le \alpha_{2\max,1}$. These lower and upper bounds of both α_1 and α_2 must be properly guessed to ensure that the first searching domain was vast enough to cover the appropriate values of α_1 and α_2. The first searching domain was next discretized with selected values of $\Delta\alpha_{1,1}$ and $\Delta\alpha_{2,1}$, resulting in a coarse

searching grid. Next, a pair of α_1 and α_2 was picked from this coarse searching grid to create the Taylor bubble shape for a computational domain with Eq.(2.2) and Eq.(2.3). Next, a flow simulation was begun until its steady-state results were obtained. So far a distribution of liquid pressure on the Taylor bubble surface, which was a result of the flow simulation, was obtained for being substituted to Eq.(2.4) in order to calculate a distribution of the gas pressure inside the Taylor bubble. Next, Eq.(2.6) was used to calculate the corresponding RMSD_p of this pair of α_1 and α_2. Then, another pair of α_1 and α_2 was picked from the coarse searching grid and the procedure was repeated until all the pairs of α_1 and α_2 from the coarse searching grid were selected. At this point, all the values of RMSD_p in the coarse searching grid were known. The minimum RMSD_p would briefly indicate the appropriate pair of α_1 and α_2 for creating the Taylor bubble shape. If more accuracy of the appropriate pair of α_1 and α_2 was not sufficient, a finer searching grid, bounded in $\alpha_{1\min,2} \le \alpha_1 \le \alpha_{1\max,2}$ and $\alpha_{2\min,2} \le \alpha_2 \le \alpha_{2\max,2}$, would be created with $\Delta\alpha_{1,2} \approx 0.5\Delta\alpha_{1,1}$ and $\Delta\alpha_{2,2} \approx 0.5\Delta\alpha_{2,1}$. The new lower and upper bounds were set as follows: $\alpha_{1\min,2} = \alpha_{1app,1} - \Delta\alpha_{1,1}$, $\alpha_{1\max,2} = \alpha_{1app,1} + \Delta\alpha_{1,1}$, $\alpha_{2\min,2} = \alpha_{2app,1} - \Delta\alpha_{2,1}$ and $\alpha_{2\max,2} = \alpha_{2app,1} + \Delta\alpha_{2,1}$. After the finer searching grid was created, the searching process would be repeated. If the accuracy of the appropriate pair of α_1 and α_2 was still not sufficient, another finer searching grid with smaller $\Delta\alpha_1$ and $\Delta\alpha_2$, would be needed. In this work, the accuracy of the appropriate pair of α_1 and α_2 was accepted when their third significant was unchanged. The flow chart of the procedure was the same as the flow chart, presented in [23].

3. Results

Table 2 presents the appropriate values of α_1 and α_2, obtained from the simulations for each condition of μ_l in accordance with Tab.1. These values of α_1 and α_2 can be employed to create the Taylor bubble shapes as shown in Fig.2a for comparison. It was apparent that (i) the less μ_l was, the thicker the shape of a Taylor bubble was; and (ii) Dumitrescu's model gave the thickest shape of the Taylor bubble in this work. Figure 2b magnifies the wall region in order to make the comparisons more evident. It was found that the obtained result agreed well with the results of [1, 5, 24].

Table 2. Appropriate values of α_1 and α_2 for each μ_l.

μ_l (Pa·s)	α_1	α_2
0.0100	*2.36*	*-7.50*
0.0075	*2.19*	*-7.80*
0.0050	*1.97*	*-8.70*
0.0025	*1.71*	*-11.0*
0.0010	*1.44*	*-14.5*

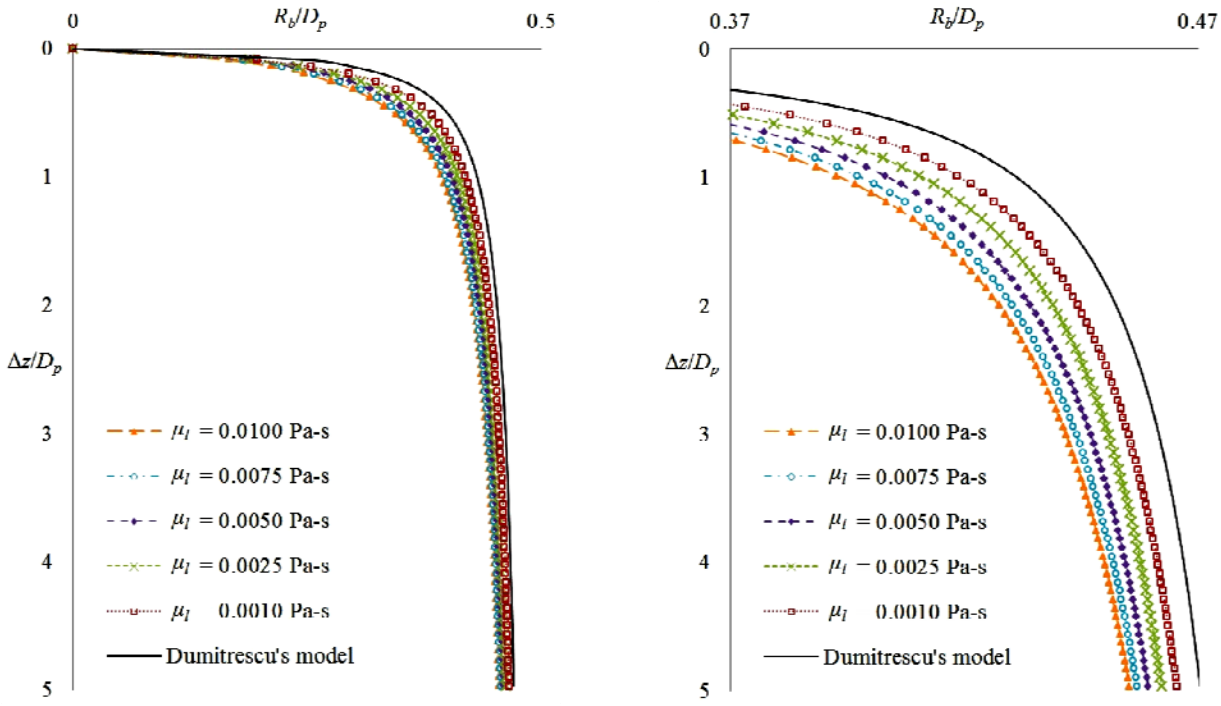

(a) Whole body (b) Wall region

Fig.2. Influence of μ_l on shapes of air Taylor bubbles in stagnant liquids with a constant $\mathrm{Fr_D} \approx 0.35$.

4. Discussion

The influence of the liquid viscosity on the Taylor bubble shape might be clarified with the theory of the log-law velocity profile, which divides a velocity profile close to a wall region to subregions. The u^+ within the viscous sublayer and the log-law region could be respectively modelled as follows [9]

$$u^+ = n^+, \tag{4.1}$$

$$u^+ = \frac{1}{\kappa}\ln\left(n^+\right) + B. \tag{4.2}$$

According to the definitions of $u^+ = |w_l|/u_\tau$ and $n^+ = \rho_l u_\tau n/\mu_l$, we could rewrite Eq.(4.1) as follows

$$\frac{|w_l|}{u_\tau} = \frac{\rho_l u_\tau n}{\mu_l},$$

$$|w_l| = \frac{\rho_l u_\tau^2 n}{\mu_l} = \frac{\tau_{wall} n}{\mu_l}, \quad \text{in which} \quad n = R_P - r. \tag{4.3}$$

The symbol of an absolute value was applied to w_l because the opposite direction of w_l with respect to the *z*-axis was omitted and only the magnitude of w_l was considered. Since the τ_{wall} was likely to be constant within the viscous sublayer [9], Eqs (4.3) shows that

$$|w_l| \propto \frac{n}{\mu_l}. \tag{4.4}$$

This meant that the magnitude of w_l would increase more rapidly with respect to n if μ_l was reduced.

Similarly as in Eq.(4.2), the velocity profile within the log-law region could be rewritten as

$$\frac{|w_l|}{u_\tau} = \frac{1}{\kappa}\ln\left(\frac{\rho_l u_\tau n}{\mu_l}\right) + B.$$

Within this region, u_τ was modelled to be $C_\mu^{1/4}\sqrt{k_l}$. This led to

$$|w_l| = \frac{u_\tau}{\kappa}\ln\left(\frac{\rho_l u_\tau n}{\mu_l}\right) + Bu_\tau = \frac{C_\mu^{1/4}\sqrt{k_l}}{\kappa}\ln\left(\frac{\rho_l C_\mu^{1/4}\sqrt{k_l}\, n}{\mu_l}\right) + BC_\mu^{1/4}\sqrt{k_l}. \tag{4.5}$$

It shows that $|w_l|$ would increase more rapidly with respect to n if either μ_l was reduced or k_l was increased (more turbulent kinetic energy in the liquid region beyond the pipe wall). It, thus, might be concluded that the magnitude of $|w_l|$ would increase more rapidly with respect to n if μ_l was reduced, similar to what happened in the viscous sublayer. As a result of this, the average value of $|w_l|$ at a cross-sectional area in the falling film ($|\overline{w}_l|$) would be increased if μ_l was reduced.

By applying a mass-flux balance between a plane far ahead of the Taylor bubble and a plane located at the fully developed film, with respect to the nose of the Taylor bubble, we got

$$\rho_l |w_t| \pi R_p^2 = \rho_l |\overline{w}_l| \pi\left(R_p^2 - R_b^2\right). \tag{4.6}$$

By substituting Eq.(1.3) into Eq.(4.6), we got

$$\rho_l \left|\mathrm{Fr_D}\sqrt{2gR_p}\right| \pi R_p^2 = \rho_l |\overline{w}_l| \pi\left(R_p^2 - R_b^2\right). \tag{4.7}$$

Assuming that ρ_l, g, R_P and $\mathrm{Fr_D}$ were constant, the derivative of Eq.(4.6) with respect to R_b yielded

$$0 = \rho_l \pi\left(R_p^2 - R_b^2\right)\frac{d|\overline{w}_l|}{dR_b} - 2\rho_l \pi |\overline{w}_l| R_b \frac{dR_b}{dR_b},$$

$$\frac{dR_b}{d|\overline{w}_l|} = \frac{R_p^2 - R_b^2}{2|\overline{w}_l| R_b} > 0 \text{ ; always.} \tag{4.8}$$

Equation (4.8) revealed that R_b would increase if $|\bar{w}_l|$ increased. Since it was already known from Eq.(4.4) and Eq.(4.5) that $|\bar{w}_l|$ would be increased if μ_l was reduced, it could be concluded that R_b would increase (the Taylor bubble would be fatter) if μ_l was reduced. This agreed well with the results in Fig.(2).

5. Conclusion

Owing to the simulated results and the analysis, regarding to the theory of the log-law velocity profile, the influence of the liquid viscosity was eventually found; namely, a higher viscosity made the shape of a Taylor bubble to be slenderer when $\mathrm{Fr_D}$ was approximately equal to *0.35*. This was the reason why Dumitrescu's model overestimated the shape of a Taylor bubble because it was derived by assuming that the liquid flow around a Taylor bubble was inviscid. The appropriate shape of a Taylor bubble could be created by using the proposed model, consisting of Eq.(2.2), Eq.(2.3) and the values of of α_1 and α_2 in Tab.2.

However, the proposed model had a defect when $0 < \Delta z / D_p < 0.033$ because it gave an imaginary number. This problem could be solved by employing an interpolation algorithm which gives an acceptable error in this narrow interval [22].

Nomenclature

D – diameter
Eo – Eötvös number
Fr – Froude number
g – gravity acceleration
L – length
M – Morton number; $\mathrm{M} = \left[\left(\rho_l - \rho_g\right) g \mu_l^4\right] \Big/ \left(\rho_l^2 \sigma^3\right)$
n – unit normal vector
p – static pressure
R – radius or radius of curvature
r – location on r-axis or correlation coefficient
Re – Reynolds number
RMSD – Root-mean-square deviation
s – slug
u – velocity component on r-axis
V – total velocity
w – velocity component on z-axis
$\bar{w}$ – area-averaged w
z – location on z-axis
Δz – distance from bubble nose; $\Delta z = z_{nose} - z$
δ – small constant or film thickness
μ – viscosity
ρ – density
σ – surface tension

Superscripts and Subscripts

app – appropriate
b – Taylor bubble
bs – Taylor bubble surface
D – diameter

film – falling film
g – gas
l – liquid
nose – Taylor bubble nose
p – pipe
t – terminal
wall – pipe wall

References

[1] Nogueira S., Riethmuler M.L., Campos J.B.L.M. and Pinto A.M.F.R. (2006): *Flow in the nose region and annual film around a Taylor bubble rising through vertical columns of stagnant and flowing Newtonian liquids*. – Chemical Engineering Science, vol.61, pp.845-857.

[2] Dumitrescu D.T. (1943): *Strömung an Einer Luftblase im Senkrechten Rohr*. – Zeitschrift fur An-gewandte Mathematik und Mechanik, vol.23, pp.139-149.

[3] Bugg J.D., Mack K. and Rezkallah K.S. (1998): *A numerical model of Taylor bubbles rising through stagnant liquids in vertical tubes*. – International Journal of Multiphase Flow, vol.24, No.2, pp.271-281.

[4] Mao Z-S. and Dukler A.E. (1990): *The motion of Taylor bubbles in vertical tubes. I. A numerical simulation for the shape and rise velocity of Taylor bubbles in stagnant and flowing liquid*. – Journal of Computational Physics, vol.91, No.1, pp.132-160.

[5] Mao Z-S. and Dukler A.E. (1991): *The motion of Taylor bubbles in vertical tubes-II. Experimental data and simulations for laminar and turbulent flow*. – Chemical Engineering Science, vol.46, No.8, pp.2055-2064.

[6] Smith S., Taha T. and Cui Z. (2002): *Enhancing hollow fibre ultrafiltration using slug-flow – a hydrodynamic study*. – Desalination, vol.146, pp.69-74.

[7] Taha T. and Cui Z.F. (2004): *Hydrodynamics of slug flow inside capillaries*. – Chemical Engineering Science, vol.59, pp.1181-1190.

[8] Thulasidas T.C., Abraham M.A. and Cerro R.L. (1997): *Flow patterns in liquid slugs during bubble-train flow inside capillaries*. – Chemical Engineering Science, vol.52, pp.2947-2962.

[9] Van Baten J.M. and Krishna R. (2004): *CFD simulation of mass transfer from Taylor bubbles rising in circular capillaries*. – Chemical Engineering Science, vol.59, pp.2535-2545.

[10] Hayashi K., Kurimoto R. and Tomiyama A. (2011): *Terminal velocity of a Taylor drop in a vertical pipe*. – International Journal of Multiphase Flow, vol.37, pp.241-251.

[11] White E.T. and Beardmore R.H. (1962): *The velocity of rise of single cylindrical air bubbles through liquids contained in vertical tubes*. – Chemical Engineering Science, vol.17, No. 5, pp.351-361.

[12] Ahmad W.R., DeJesus J.M. and Kawaji M. (1998): *Falling film hydrodynamics in slug flow*. – Chemical Engineering Science, vol.53, pp.123-130.

[13] Hout R.V., Bernea D. and Shemer L. (2001): *Evolution of statistical parameters of gas-liquid slug flow along vertical pipes*. – International Journal of Multiphase Flow, vol.27, pp.1579-1602.

[14] Pinto A.M.F.R., Coelho Pinheiro M.N. and Campos J.B.L. (2001): *On the interaction of Taylor bubbles rising in two-phase co-current slug flow in vertical columns: turbulent wakes*. – Experiments in Fluids, vol.31, pp.643-652.

[15] Kytömaa H.K. and Brennen C.E. (1991): *Small amplitude kinematic wave propagation in two-component media*. – International Journal of Multiphase Flow, vol.17, No.1, pp.13-26.

[16] Cheng H., Hills J.H. and Azzorpardi B.J. (1998): *A study of the bubble-to-slug transition in vertical gas-liquid flow in columns of different diameter*. – International Journal of Multiphase Flow, vol.24, No.3, pp.431-452.

[17] Sun B., Wang R., Zhao X. and Yan D. (2002): *The mechanism for the formation of slug flow in vertical gas-liquid two-phase flow*. – Solid-State Electronics, vol.46, No.12, pp.2323-2329.

[18] Mayor T.S., Pinto A.M.F.R. and Campos J.B.L.M. (2007): *Hydrodynamics of gas-liquid slug flow along vertical pipes in the laminar regimes-experimental and simulation study*. – Industrial and Engineering Chemistry Research, vol.46, pp.3794-3809.

[19] Ferziger J.H. and Peric M. (2002): *Computational Methods for Fluid Dynamics*. – Germany: Springer.

[20] Hout R.V., Bernea D. and Shemer L. (2003): *Evolution of hydrodynamic and statistical parameters of gas-liquid slug flow along inclined pipes*. – Chemical Engineering Science, vol.58, No.1, pp.115-133.

[21] Shemer L. (2003): *Hydrodynamic and statistical parameters of slug flow*. – International Journal of Heat and Fluid Flow, vol.24, pp.334-344.

[22] Lertnuwat B. (2015): *Model for predicting the head shape of a Taylor bubble rising through stagnant liquids in a vertical tube*. – Thammasat International Journal of Science and Technology, vol.20, No. 1, pp.37-46.

[23] Lertnuwat B. (2018): *Shapes of an air Taylor bubble in stagnant liquids influenced by different surface tensions*. – International Journal of Applied Mechanics and Engineering. vol.23, No.1, pp.79-90.

[24] Salakij S. and Lertnuwat B. (2018): *Influence of viscosity on the shape of an air Taylor bubble in a stagnant liquid under laminar condition in falling film region*. – International Journal of Applied Engineering Research, vol.13, No.1, pp.8-13.

Received: May 1, 2018

Revised: June 26, 2018